Journal of Engineering and Sustainable Development
Vol. 30, No. 02, March 2026
https://jeasd.uomustansiriyah.edu.iq/index.php/jeasd
ISSN 2520-0917
Research Article
https://doi.org/10.31272/jeasd.2233

Tri-Band Two Rings Antenna Loaded with Inter-Digital Capacitor for Fifth Generation Applications

Nada N. Tawfeeq*, Adheed H. Sallomi

Electrical Engineering Department, College of Engineering, Mustansiriyah University, Baghdad, Iraq

*Email: nada.nasih@uomustansiriyah.edu.iq

Article Info

Received	**20/09/2024**
Revised	**23/09/2025**
Accepted	**23/09/2025**

Abstract

For fifth-generation applications, a tri-band antenna loaded with an inter-digital capacitor is suggested in this study. The antenna consists of two hexagonal rings connected to a capacitor and a partially rectangular ground plane, which is fed by a 50 Ohm microstrip transmission line. The tri-band characteristics of the antenna are achieved through the combination of the capacitor design and the hexagonal patch on the ground plane, which alters the current flow. The suggested antenna has dimensions of 7.6 x 10.5 x 0.8 mm³ and is constructed on a Roger 5880 substrate with a height of 0.8 mm, a relative dielectric constant of 2.2, and a loss tangent of 0.0009. The findings of the study demonstrate that the antenna exhibits three bandwidths suitable for 5G applications. These include bandwidths of 3.5 GHz (12.7% from 25.8 GHz to 29.3 GHz), 4.6 GHz (11.7% from 36.9 GHz to 41.5 GHz), and 14.3 GHz (25.3% from 49.3 GHz to 63.6 GHz). The antenna achieves resonance frequencies of 28 GHz, 38 GHz, and 60 GHz for these three respective bandwidths. Moreover, the suggested compact antenna demonstrates reasonable gain and an omnidirectional radiating pattern, making it suitable for use in mobile handsets.

Keywords: Fifth Generation; Inter-digital capacitor; Omnidirectional; Ring; Tri band

1. Introduction

The future fifth generation (5G) of mobile communications systems is predicted to significantly increase system performance in general, such as data transmission speeds and energy usage [1],[2]. Studies in the past have suggested many forms of millimeter wave (mmW) antenna designs that operate at single or multiple operating frequency bands with inventive designs or construction techniques. A single-frequency sub-6 GHz four-port antenna of 4 GHz bandwidth, omnidirectional pattern, and acceptable gain for MIMO applications has been proposed [3]. The two element array with expanded structure and substrate integrated waveguide (SIW) technology was utilized to create the directional horn antenna operating at 26 GHz as a transmitter with maximum gain of 8 dB with dimensions 28.2 x 28.6 mm^2 [4]. Also, another antenna with a fundamental frequency of 26 GHz but a different design technique of a rectangular dielectric resonator antenna fed by a circular patch has been proposed [5]. The design is compact, with dimensions 5.76 x 5.76 mm2 and a high directional gain of 8.04 dB. Patch antennas operating at 28 GHz bands have also been suggested, including a 4-element array vivaldi antenna [6], circularly polarized planar helix phased antenna array of 7 GHz bandwidth and 5 dB gain [7], and directional patch loaded with slot of H shape along a shorting-pin construction with high gain of 12 dB but large dimensions of 96.6 x 96.6 mm^2 [8]. New structures can achieve a high directional gain of 27 dBi at 28 GHz, which involves the superimposed similar metal sheets founded on metasurfaces of large size 160 x 160 x 140 mm^3[9]. In the frequency band of 60 GHz, a stacked aperture-coupled directional microstrip patch antenna (MPA) with a grid-based parasitic patch of 40 x 20 mm^2 compact size and 8 dB gain [10]. Electromagnetic Bandgap (EBG), including the cross metallic, hexagonal, and mushroom pattern periodic structures [11]. Q and double F slots loaded patch with microstrip feeder structure [12],[13], and a four-element regular patch antenna with Z-shaped slots on the ground plane [14] have also been proposed in patch antennas. All the slot antennas mentioned showed a gain range of (6-12) dB and a compact size. Another shape of slot is used with electronic switches, as proposed in [15], where two electronic switches are on a 5.4 x 5.4 mm2 patch used to produce triple distinct beam configurations with a maximum gain of 4.9 dB. Using either switch separately leads to a 70° change in the central radiation pattern path within similar band properties.

All the mentions above regard an mm-wave antenna that covers a single operating band. Other designs are focused on covering

dual operating bands or higher. The authors suggest an efficient MPA that operates in two bands, 38 and 60 GHz, with a new design consisting of dual patches connected by electromagnetic force, which incorporates sophisticated radiating processes [16]. A directional patch antenna in the shape of an umbrella has been proposed to resonate throughout three frequency bands, 28, 38, and 55 GHz [17]. Others are aimed at getting a great gain. A frequency-selective surface (FSS) array antenna is suggested in [18], where the design consists of 8 sub-antennas supplied by one feeder and an FSS that has 84 unit cells. The wide band antenna covers mm-wave 5G bands that include 28, 38, and 60 GHz, and has a gain of 15 dB. In this article, a two-ring microstrip patch antenna loaded with an interdigital capacitor (IDC) is proposed. The implementation of the capacitor and ground plane extensions results in tri-bands with a more effective return loss characteristic. For fifth-generation uses, the antenna is intended to operate at 28, 38, and 60 GHz. The CST Studio Suite® software program was used to carry out the electromagnetic simulations.

2. Method of the Research

2.1 Antenna Configuration and Substrate Selection

The proposed antenna is a compact tri-band microstrip monopole structure designed to operate at 28 GHz, 38 GHz, and 60 GHz for fifth-generation (5G) applications. The antenna is fabricated on a Rogers RT/duroid 5880 substrate with the following characteristics: relative dielectric constant: $\varepsilon r = 2.2$, Loss tangent: 0.0009, Substrate thickness: 0.8 mm, and Overall substrate dimensions: 7.6×10.5 mm^2

The radiating element consists of two concentric hexagonal rings connected through an inter-digital capacitor (IDC). The antenna is fed by a 50 Ω microstrip transmission line incorporating a quarter-wave impedance transformer for proper matching. A partial ground plane is used to enhance impedance bandwidth and support monopole-type radiation behavior.

Fig. 1 depicts the shape of the proposed tri-band microstrip patch antenna, where S1 and S2 denote the length of the hexagon patch sides of the first and second rings. The distance between the two rings is denoted by Sd. Additionally, the width of the inter-digital capacitor base is D, and the length of the IDC finger is Ld. The feed-line consists of two sections: the main feeder of length Lf and width Wf, and the quarter-wave transformer whose dimensions are Lq and Wq for length and width, respectively. Lastly, Lg and Wg refer to the partial ground plane's length and width. Lg1 and Sg are the dimensions of the extension of the ground plane. The dimensions of all components are listed in Table 1 and Fig.1.

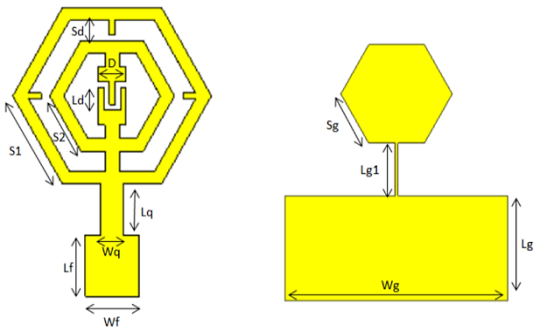

Figure 1. The two rings tri-band (28/38/60 GHz) MPA geometries

Table 1. Parameters of the proposed tri-band antenna

Dimension	Value (mm)	Dimension	Value (mm)
S1	3.5	Lf	2.1
S2	2.1	Wf	1.9
Ld	0.8	Lg	3.1
D	1	Wg	7.6
Sd	0.8	Lg1	1.75
Lq	2	Sg	1.9
Wq	0.8		

2.2 Design Evolution Procedure

The antenna design was developed through four progressive stages to achieve tri-band operation, as shown in Fig. 2 [19].

- Mode-A: A single hexagonal ring monopole fed by a microstrip line with a quarter-wave transformer over a partial ground plane, designed to resonate at 28 GHz.
- Mode-B: Addition of a second inner hexagonal ring to introduce electromagnetic coupling and generate a higher-frequency resonance.
- Mode-C: Integration of an inter-digital capacitor (IDC) between the rings to compensate for inductive reactance and improve impedance matching.
- Mode-D: Modification of the ground plane by adding hexagonal and narrow-line extensions to introduce a third operating band near 60 GHz.

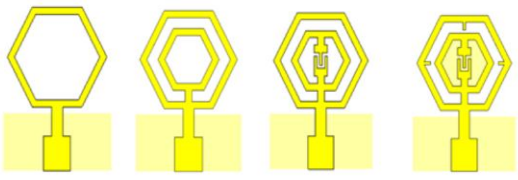

(a) (b) (c) (d)

Figure 2. Evolution of the two rings tri-band antenna: (a) Mode-A, (b) Mode-B, (c) Mode-C, (d) Mode-D

2.3 Microstrip Transmission Line Design

When the transmission-line impedance Zc is 50 Ohm, the quarter-wave transforming impedance Zt has been computed by changing Rin and Zc in (1) [20]:

$$Z_{t=}\sqrt{Z_c R_{in}} \quad (1)$$

Where Rin is the radiated patch's input impedance. Once the transmission lines' impedance values have been determined, their diameters are estimated using (2) to (5).

The transmission line width (Wt) is determined utilizing (2), (3), and (4), where Z0 refers to the transmission line section impedance to be computed [21]; throughout the case of Fig. 1, the computation for Zc and Zt must be carried out separately.

$$A = \frac{Z_0}{60}\sqrt{\frac{\varepsilon_r+1}{2}} + \frac{\varepsilon_r-1}{\varepsilon_r+1}\left(0.23 + \frac{0.11}{\varepsilon_r}\right) \quad (2)$$

Where ε_r is the dielectric constant of the substrate

$$B = \frac{377\pi}{2Z_0\sqrt{\varepsilon_r}} \quad (3)$$

$$\frac{Wt}{h} = \begin{cases} \frac{8e^A}{e^{2A}-2} & para\ \frac{Wt}{h} < 2 \\ \frac{2}{\pi}\left[B - 1 - \ln(2B-1) + \frac{\varepsilon_r-1}{2\varepsilon_r}\left\{\ln(B-1) + 0.39 - \frac{0.61}{\varepsilon_r}\right\}\right] & para\ \frac{Wt}{h} < 2 \end{cases} \quad (4)$$

In order to determine the length of the transmission line, the effective dielectric constant (ε_{reffLt}) for each transmission line is initially computed using (5):

$$\varepsilon_{reffLt} = \frac{\varepsilon_r+1}{2} + \frac{\varepsilon_r-1}{2}\frac{1}{\sqrt{1+12\frac{h}{Wt}}} \quad (5)$$

Once the effective dielectric constant has been computed, the length of the transmission line (Lt) can be determined using (6).

$$Lt = \frac{\phi f_c(\frac{\pi}{180})}{\sqrt{\varepsilon_{reffLt}}k_0} \quad (6)$$

Where φ is the phase delay, k0 is the phase constant in free space.

3. Results and Discussions

The substrate dimensions are 7.6 x 10.5 mm2. Mode-A has a single working frequency of 28.5 GHz, with a bandwidth of (26.25-29) GHz. The radiating pattern in the orthogonal elevating planes (Phi = 0◦ and Phi = 90◦) is omnidirectional owing to the partial-length ground structure. To get a second operating band at a higher frequency, another ring is added inside the main monopole ring. The S11 performance shows that the introduction of this ring added an operating band ranging from 35-41.5 GHz, at the expense of deleting the 28 GHz band. To enhance the antenna's performance, an inter-digital capacitor is positioned at the center of the monopole two-ring antenna, as demonstrated in Mode B.

Fig. 3 depicts the Mode-C reflection coefficient; it can be observed that the Mode-B antenna displays inductive reactance when operating at 28 GHz. In order to enhance the impedance matching, an inter-digital capacitor (IDC) has been added as shown in Figure 2-c. The antenna's reactance impedance at 28 GHz is 22.9+j5.06 Ω without the IDC.

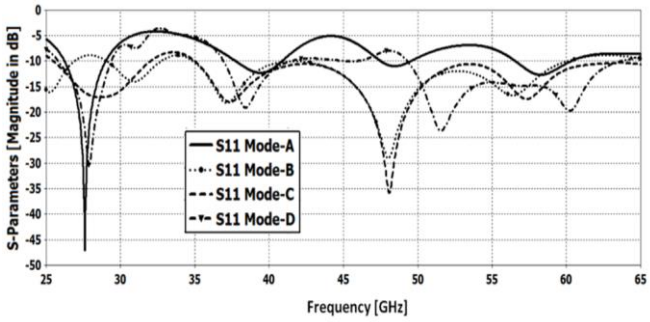

Figure 3. Reflection coefficients of the two-ring tri-band design modes

However, after implementing the IDC, the reactance impedance can be effectively reduced to 60.1-10.7 Ω, leading to better impedance matching. The capacitance of the inter-digital capacitor is computed to be 0.019 pF using (7) from [22] as shown in Fig 4.

$$C = (\varepsilon_r + 1)l[(N-3)A_1 + A_2] \qquad (pF) \qquad (7)$$

The length of each finger is represented by "l", and the number of fingers is denoted by "N". The capacitances per unit length of the fingers on the interior, exterior 1, and exterior 2 are indicated by "A_1" and "A_2", respectively.

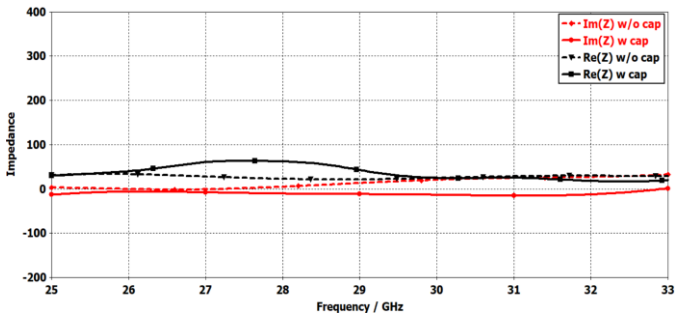

Figure 4. Comparison of Antenna impedances as a function of frequency with and without the capacitor implemented

In the proposed design, the finger width is uniform, and its length is less than or equal to λ/4. Since the substrate is finite, the impact of the substrate's thickness, "h", must be taken into account when determining A_1 and A_2 in pF/μm, and the approximate expressions are presented below in (8) and (9) [23]:

$$A_1 = 4.409 \tanh\left[0.55\left(\frac{h}{W_{IDC}}\right)^{0.45}\right] \text{x} 10^{-6} \quad (8)$$

$$A_2 = 9.92 \tanh\left[0.52\left(\frac{h}{W_{IDC}}\right)^{0.5}\right] \text{x} 10^{-6} \quad (9)$$

By incorporating a capacitor, a good impedance matching in the 28 GHz band is achieved, thereby introducing the dual operating bands of 28 and 38 GHz. As for the 60 GHz band, it suffers from poor S11. In order to achieve the third operating frequency at the higher end, two extensions of a shape hexagonal patch and a narrow line in the ground plane are added, as shown in Mode-D. Further stubs of dimensions (0.44 mm x 0.2 mm) were added to the external ring patch to enhance the gain of the antenna.

The simulated current distributions of the proposed antenna through the design stages are shown in Fig. 5. The effect of adding an interdigital capacitor on the antenna behavior at 28 GHz is shown in Fig. 5 (a) and (b). It is noticed that by adding IDC, the current will concentrate in the rings and through the capacitor. The patch on the backside did not affect the current on the front side as shown in (c). On the other hand, the current distribution at 38 GHz is barely affected by the presence of the capacitor and ground patch, as shown in (d), (e), and (f). As for 60 GHz, it can be noticed that the capacitor did not affect the current in (g) and (h). However, the addition of the patch on the ground plane induced the current to distribute through the inner ring and the ground patch in (i).

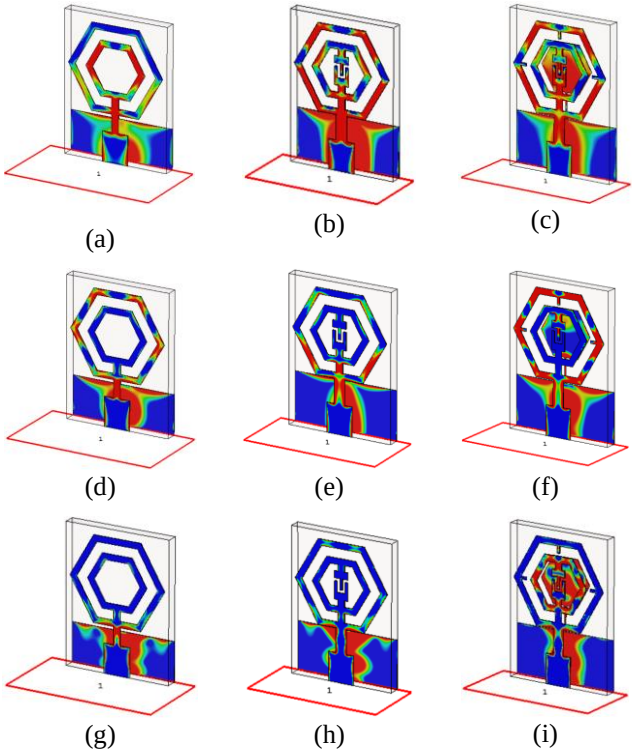

Figure. 5. Current distribution of tri-band dual ring antenna: (a), (b) and (c) at 28 GHz in Modes-B, C and D (d), (e) and (f) at 38 GHz in Modes-B, C and D (g), (h) and (i) at 60 GHz in Modes-B, C and D

The gain is plotted against frequency in Fig. 6. It is observed that at the 28 GHz band, a maximum peak gain of 4.3 dB is achieved. Meanwhile, at the 38 GHz band, the gain reached 4.5 dB. Finally, a high gain of 7.4 dB has been achieved within the 60 GHz band.

A comparison of the radiation pattern in the E-plane and H-plane is shown in Fig. 7. An omnidirectional pattern is obtained in all operating bands.

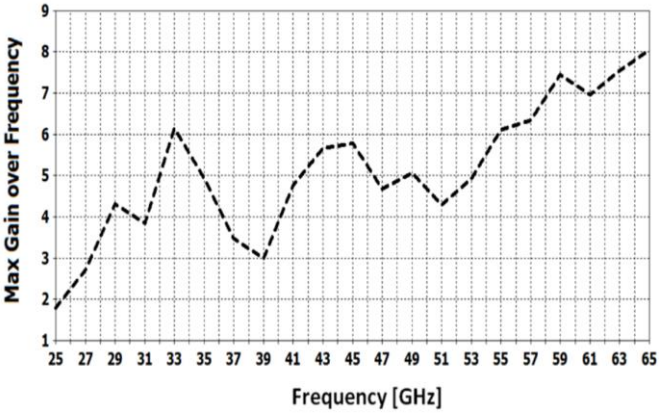

Figure 6 Gain against frequency at: (a) 28 GHz band, (b) 38 GHz band, (c) 60 GHz band

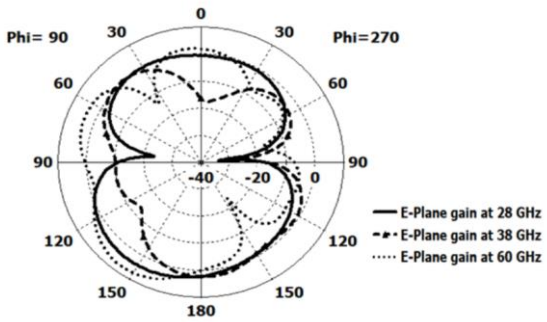

(a)

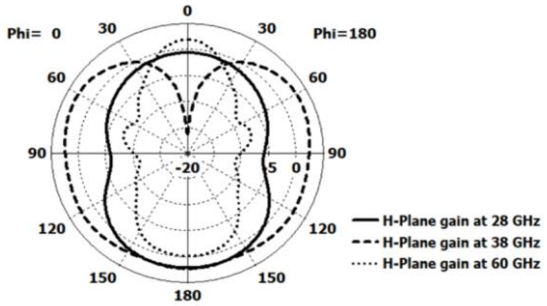

(b)

Figure 7. Comparison of radiation patterns at 28 GHz, 38 GHz, and 60 GHz in: (a) E-Plane, (b) H-plane.

4. Conclusion

A tri-band monopole antenna loaded with IDC is proposed in this study. The proposed antenna is developed on a 79.8 mm^2 Roger 5880 substrate. The electromagnetic radiation characteristics are endorsed by the CST Studio Suite® software program. The IDC loaded in the proposed design gives the ability to operate at two frequencies. The addition of the hexagonal patch on the ground plane introduced a third band. Further stubs are added to the external ring of the radiating patch to improve the gain. The proposed design shows steady radiating patterns for both E and H planes within the three operating frequencies. The proposed antenna system covers a large spectrum from (25.8-29.3) GHz, (36.9-41.5) GHz to (49.3-63.6) GHz, which includes three possible frequencies for 5G communications in the 28, 38, and 60 GH bands. In addition to the fact that it offers advantages such as small size, large bandwidth, facilitated fabrication, and acceptable gain values at the intended bands of 28, 38, and 60 GHz. Because the electromagnetic radiation is omnidirectional, the suggested antenna is an attractive choice for inclusion in an array for future 5 G applications.

Acknowledgements

This work is supported by the College of Engineering/ Mustansiriyah University.

Conflict of interest

The authors declare that there are no conflicts of interest regarding the publication of this manuscript.

Author Contribution Statement

Both Authors proposed the study problem, performed the computations, and supervised the findings of this work. Also, both discussed the results and contributed to the final manuscript.

References

[1] T. L. Marzetta, "Massive MIMO for next generation wireless systems," *IEEE Communications Magazine*, vol. 52, no. 2, pp. 186–195, Feb. 2014. doi: https://doi.org/10.1109/MCOM.2014.6736761

[2] E. Björnson, J. Hoydis, and L. Sanguinetti, "Massive MIMO networks: Spectral, energy, and hardware efficiency," *Foundations and Trends® in Signal Processing*, vol. 11, nos. 3–4, pp. 154–655, 2017. doi: https://doi.org/10.1561/2000000093

[3] M. Salamin and H. Niamat, "A wideband 4-port MIMO antenna supporting sub-6 GHz spectrum for 5G mobile terminals," *Frequenz*, vol. 76, pp. 45–54, 2021. doi: https://doi.org/10.1515/freq-2021-0070.

[4] T. Hong, S. L. Zheng, R. K. Liu, and W. T. Zhao, "Design of mmWave directional antenna for enhanced 5G broadcasting coverage," *Sensors*, vol. 21, no. 3, p. 746, 2021. doi: https://doi.org/10.3390/s21030746.

[5] A. S. Dixit, S. Kumar, S. Urooj, and A. Malibari, "A highly compact antipodal Vivaldi antenna array for 5G millimeter wave applications," *Sensors*, vol. 21, no. 7, p. 2360, 2021. doi: https://doi.org/10.3390/s21072360.

[6] I. Syrytsin, S. Zhang, and G. Fr, "Circularly polarized planar helix phased antenna array for 5G mobile terminals," in *Proc. Int. Conf. on Electromagnetics in Advanced Applications (ICEAA)*, 2017, pp. 1105–1108.doi:https://doi.org/10.1109/ICEAA.2017.8065458.

[7] Y. J. Kim, Y. B. Kim, and H. L. Lee, "mmWave high-gain planar H-shaped shorted ring antenna array," *Sensors*, vol. 20, no. 18, pp. 51–68, 2020. doi: https://doi.org/10.3390/s20185168.

[8] Gaya, A., Jamaluddin, M.H., Ali, I. Althuwayb, A.A. (2021). Circular Patch Fed Rectangular Dielectric Resonator Antenna with High Gain and High Efficiency for Millimeter Wave 5G Small Cell Applications. Sensors, Vol. 21, p. 2694.https://doi.org/10.3390/s21082694.

[9] A. Gaya, M. H. Jamaluddin, I. Ali, and A. A. Althuwayb, "Circular patch-fed rectangular dielectric resonator antenna with high gain and high efficiency for millimeter-wave 5G small cell applications," *Sensors*, vol. 21, no. 8, p. 2694, 2021. doi: https://doi.org/10.3390/s21082694.

[10] A. Bondarik and D. Sjöberg, "Microstrip antenna with beam shift capability for 60 GHz band," *Progress In Electromagnetics Research B*, vol. 62, pp. 319–331, 2015. doi: https://doi.org/10.2528/PIERB15012303.

[11] W. E. McKinzie, D. M. Nair, B. A. Thrasher, M. A. Smith, E. D. Hughes, and J. M. Parisi, "60-GHz 2 × 2 LTCC patch antenna array with an integrated EBG structure for gain enhancement," *IEEE Antennas and Wireless Propagation Letters*, vol. 15, pp. 1522–1525, 2016. doi:https://doi.org/10.1109/LAWP.2016.2517141.

[12] M. Khan, K. Islam, N. Shovon, M. Baz, and M. Masud, "Design of a novel 60-GHz millimeter-wave Q-slot antenna for body-centric communications," *International Journal of Antennas and Propagation*, vol. 2021, Article ID 9795959, 12 pages, 2021. doi: https://doi.org/10.1155/2021/9795959.

[13] F. Ahmad and B. Tlili, "Design and analysis of millimeter-wave double F-slot patch antenna for future 5G wireless communication," in *Proc. Int. Conf. on Electrical and Computing Technologies and Applications (ICECTA)*, 2017, pp. 1–4. doi: https://doi.org/10.1109/ICECTA.2017.8252049.

[14] S. Ullah, W. H. Yeo, and H. Kim, "Development of 60-GHz millimeter-wave electromagnetic bandgap ground planes for multiple-input multiple-output antenna applications," *Scientific Reports*, vol. 10, p. 8541, 2020. doi: https://doi.org/10.1038/s41598-020-65622-9.

[15] Y. I. Al-Yasir, H. A. Al-Behadili, B. A. Sawadi, N. O. Parchin, A. M. Abdulkhaleq, A. S. Abdullah, and R. A. Abd-Alhameed, "New radiation pattern-reconfigurable 60-GHz antenna for 5G communications," in *Modern Printed-Circuit Antennas*, IntechOpen, 2019.doi: https://doi.org/10.5772/intechopen.88167.

[16] M. H. A. I. Sharaf, R. K. Zaki, M. M. Omar, and R. K. Hamad, "A novel dual-band (38/60 GHz) patch antenna for 5G mobile handsets," *Sensors*, vol. 20, no. 9, p. 2541, 2020. doi: https://doi.org/10.3390/s20092541.

[17] M. Hussain, S. Jarchavi, S. Naqvi, U. Gulzar, S. Khan, M. Alibakhshikenari, and I. Huynen, "Design and fabrication of a printed tri-band antenna for 5G applications operating across Ka- and V-band spectrums," *Electronics*, vol. 10, no. 21, p. 2674, 2021. doi: https://doi.org/10.3390/electronics10212674.

[18] R. Ullah, "Wideband and high-gain array antenna for 5G smartphone applications using frequency selective surface," *IEEE Access*, vol. 10, pp. 86117–86126, 2022. doi: https://doi.org/10.1109/ACCESS.2022.3196687.

R. S. Daniel, R. Pandeeswari, and S. Raghavan, "Dual-band monopole antenna loaded with ELC metamaterial resonator for WiMAX and WLAN applications," *Applied Physics A*, vol. 124, p. 570, 2018. doi: https://doi.org/10.1007/s00339-018-1985-7.

[19] C. A. Balanis, *Antenna Theory: Analysis and Design*, 4th ed., Hoboken, NJ, USA: John Wiley & Sons, 2016, pp. 783–867.

[20] J. C. Martínez Quintero, E. P. Estupiñán Cuesta, and G. L. Escobar Quiroga, "Design, analysis, and simulation of 60 GHz millimeter-wave MIMO microstrip antennas," *Journal of Sensor and Actuator Networks*, vol. 11, no. 4, p. 59, 2022. doi: https://doi.org/10.3390/jsan11040059

[21] G. D. Alley, "Interdigital capacitors and their application in lumped-element microwave integrated circuits," *IEEE Transactions on Microwave Theory and Techniques*, vol. 18, no. 12, pp. 1028–1033, 1970. doi: https://doi.org/10.1109/TMTT.1970.1127407.

[22] J. Ghimire and D. Y. Choi, "Design of a compact ultrawideband U-shaped slot etched on a circular patch antenna with notch characteristics for ultrawideband applications," *International Journal of Antennas and Propagation*, vol. 2019, Article ID 8090936, 2019. https://doi.org/10.1155/2019/8090936